Automatic segmentation of intravital fluorescence microscopy images by K-means clustering of FLIM phasors

YIDE ZHANG[1,4], TAKASHI HATO[2], PIERRE C. DAGHER[2], EVAN L. NICHOLS[3], CODY J. SMITH[3], KENNETH W. DUNN[2], AND SCOTT S. HOWARD[1,*]

[1] Department of Electrical Engineering, University of Notre Dame, Notre Dame, IN 46556, USA
[2] Department of Medicine, Division of Nephrology, Indiana University, Indianapolis, IN 46202, USA
[3] Department of Biological Sciences, University of Notre Dame, Notre Dame, IN 46556, USA
[4] e-mail: yzhang34@nd.edu
[*] Corresponding author: showard@nd.edu

Compiled July 11, 2019

Fluorescence lifetime imaging microscopy (FLIM) provides additional contrast for fluorophores with overlapping emission spectra. The phasor approach to FLIM greatly reduces the complexity of FLIM analysis and enables a useful image segmentation technique by selecting adjacent phasor points and labeling their corresponding pixels with different colors. This phasor labeling process, however, is empirical and could lead to biased results. In this Letter, we present a novel and unbiased approach to automate the phasor labeling process using an unsupervised machine learning technique, i.e., K-means clustering. In addition, we provide an open-source, user-friendly program that enables users to easily employ the proposed approach. We demonstrate successful image segmentation on 2D and 3D FLIM images of fixed cells and living animals acquired with two different FLIM systems. Finally, we evaluate how different parameters affect the segmentation result and provide a guideline for users to achieve optimal performance.

http://dx.doi.org/10.1364/ao.XX.XXXXXX

Fluorescence lifetime imaging microscopy (FLIM) is an important technique in biomedical research as it measures the fluorescence decay rate of fluorophores and uses it to provide additional contrast to a fluorescence intensity image [1]. FLIM is particularly powerful because many fluorophores have overlapping emission spectra. Features that cannot be separated on a conventional fluorescence microscopy image, such as the two-photon fluorescence intensity image of mouse kidney *in vivo* shown in Fig. 1(a), can be segmented based on their lifetime contrast [Fig. 1(b)]. However, the measured lifetime at a pixel is an average value and it cannot resolve the heterogeneity of fluorophores at that pixel, as different fluorophore compositions (single fluorophore, multiple fluorophores) or excited state reactions could result in the same average lifetime measurement. The phasor approach is a coordinate transformation that directly transforms the fluorescence decay in an image to a phasor plot, where the coordinates (g as the x-coordinate, and s as the y-coordinate) of each phasor point efficiently encode the fluorescence decay information of its corresponding pixel in the image [Fig. 1(c)] [2–4]. Different fluorophore compositions and possible excited state reactions can alter the phasor coordinates (g and s) even if the average lifetime might be unaltered; therefore, the heterogeneity of fluorophores can be resolved with the phasor approach.

In the phasor plot, pixels with similar fluorescence decays tend to congregate and form a cluster. This feature can be used to segment the image pixels based on the similarity of their fluorescence decays. Specifically, one can select the phasor points clustered together on the phasor plot [Fig. 1(d)] and manually label their corresponding pixels in the original image with a certain color [Fig. 1(f)] [4, 5]. This phasor labeling process, however, is empirical because in most cases, especially in intravital imaging where autofluorescence is predominant, the user does not have *a priori* knowledge of the fluorophores and their lifetimes. Therefore, to segment the image properly, the user often selects regions in the phasor plot arbitrarily and meanwhile observes the corresponding labeled pixels in the original image. This process usually requires multiple trials and it could lead to biased segmentation results.

In this Letter, we present a novel and unbiased approach to automate the empirical phasor labeling process using an unsupervised machine learning technique, i.e., K-means clustering [6, 7]. By giving an estimated number, K, of different fluorophores present in the image, the approach separates its phasor plot into K clusters using the K-means algorithm [Fig. 1(e)] and automatically segments the original image into K parts by color-labeling the pixels corresponding to the K clusters [Fig. 1(g)]. With this approach, the phasors can be automatically organized into sensible groupings and the segmentation result is more reliable than that acquired empirically. In addition, we provide a user-friendly program with graphical user interface (GUI) that enables users to easily employ the proposed approach. The

This is the author's manuscript of the article published in final edited form as:
Zhang, Y., Zhang, Y., Hato, T., Dagher, P. C., Nichols, E. L., Smith, C. J., Dunn, K. W., & Howard, S. S. (2019). Automatic segmentation of intravital fluorescence microscopy images by K-means clustering of FLIM phasors. Optics Letters, 44(16), 3928–3931. https://doi.org/10.1364/OL.44.003928

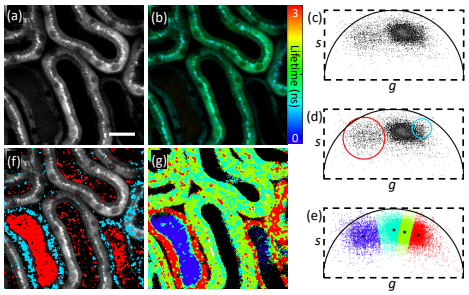

Fig. 1. The two-photon intensity image (a), fluorescence lifetime image (b), phasor plot (c), phasor labeling process (d,f), and K-means clustering on phasors (e,g) of the kidney in a living mouse. Scale bar: 20 µm.

program is open-source and can be accessed via GitHub[1]. We demonstrate successful image segmentation results with the program on 2D and 3D intravital FLIM images of mouse kidneys and zebrafish embryos acquired from two different FLIM systems. Finally, we evaluate the effect of different parameters used in the program on segmentation results and provide a guideline for users aiming to achieve optimal performance.

The phasor plot can be acquired with either a time-domain (TD) or a frequency-domain (FD) FLIM setup [8–10]. In TD-FLIM techniques, such as time-correlated single-photon counting (TCSPC), the phasor plot is obtained by transforming the histogram of the photon arrival time of each image pixel, $I(t)$, to phasor coordinates, g and s, by $g_i = \int_T I_i(t)\cos(\omega t)dt / \int_T I_i(t)dt$ and $s_i = \int_T I_i(t)\sin(\omega t)dt / \int_T I_i(t)dt$, where i is the index of the pixel in the image, ω is the angular frequency of excitation, and T is the pixel dwell time. In FD-FLIM approaches, phasor coordinates are obtained by $g_i = m_i \cdot \cos(\phi_i)$ and $s_i = m_i \cdot \sin(\phi_i)$, where m_i and ϕ_i are the modulation degree change and phase shift, respectively, of the emission with respect to the excitation in the frequency-domain measurements. Regardless of whether the phasors are acquired with TD- or FD-FLIM setups, the phasor coordinates are related to the lifetimes by $g_i = \sum_k a_{k,i}/[1+(\tau_k\omega)^2]$ and $s_i = \sum_k a_{k,i}\tau_k\omega/[1+(\tau_k\omega)^2]$, where $a_{k,i}$ is the intensity-weighted fractional contribution of the fluorophore with lifetime τ_k at the i-th pixel and $\sum_k a_{k,i} = 1$.

The provided open-source GUI program was written in Matlab (MathWorks). One can import the imaging data from their existing FLIM setup to our program by (1) saving the phasor and intensity images to TIFF or CSV files and (2) loading the phasor (g and s) and intensity images into the program. Once the data are imported, the program can generate a fluorescence (phase) lifetime image by calculating the average lifetime value on each pixel with $\bar{\tau}_i = s_i/(g_i\omega) = \sum_k a_{k,i}\tau_k$, where $\omega = 2\pi f$ and f is the excitation modulation frequency that the user needs to specify. Note that we only consider phase-derived lifetimes in this Letter for its simpler mathematical form compared to modulation-derived lifetimes [1]. Since FLIM data usually have a low signal-to-noise ratio (SNR) [11], we provide an image filtering option in the program, such that the user can apply a median filter (3×3 or 5×5 kernels) or a smoothing filter on the phasor or intensity images, one or multiple times, to increase their SNR [4]. Note that the median filter does not decrease the resolution of the images [4]. Considering that most noise comes from pixels with low intensity, the program also allows the exclusion of pixels with intensity below a threshold to reduce noise disruption to the algorithm. To perform K-means clustering on the phasors, the user needs to specify the parameters used in the algorithm (Algorithm 1), including the number of clusters (K), the distance metric (squared Euclidean, $L1$, or cosine), and the number of times to replicate the procedure. We utilize K-means++ as a heuristic seeding technique to improve the speed and performance of the K-means algorithm [12]. Finally, when the clustering operation is completed, the user can export the segmented images into separated TIFF files.

[1] https://github.com/yzhang34/Kmeans-FLIM-Phasors.git

Algorithm 1. K-means clustering on FLIM phasors.

procedure KMEANSONPHASORS($K, dist, \vec{g}, \vec{s}$)
  $\mathbf{P} \leftarrow \{\vec{g}', \vec{s}'\}$
  $\vec{c_1} \leftarrow$ select $\vec{p} \in \mathbf{P}$ uniformly at random
  for $k \leftarrow 2, K$ **do** ▷ K-means++ algorithm
    for $j \leftarrow 1, k-1$ **do**
      if $dist =$ 'Euclidean' **then**
        $d(\vec{p}, \vec{c_j}) \leftarrow (\vec{p}-\vec{c_j})'(\vec{p}-\vec{c_j})$
      else if $dist =$ 'L1' **then**
        $d(\vec{p}, \vec{c_j}) \leftarrow |\vec{p}(1)-\vec{c_j}(1)| + |\vec{p}(2)-\vec{c_j}(2)|$
      else if $dist =$ 'Cosine' **then**
        $d(\vec{p}, \vec{c_j}) \leftarrow 1 - \frac{\vec{p}'\vec{c_j}}{(\vec{p}'\vec{p})(\vec{c_j}'\vec{c_j})}$
      $\mathbf{C_j} \leftarrow \vec{p} \in \mathbf{P}_{\vec{p}\neq\vec{c_j}}$ with $d(\vec{p}, \vec{c_j}) < d(\vec{p}, \vec{c_l})(j \neq l)$
      for all $\vec{p} \in \mathbf{C_j}$ **do**
        $D(\vec{p}) \leftarrow d(\vec{p}, \vec{c_j})$
    $\vec{c_k} \leftarrow$ select $\vec{p} \in \mathbf{P}$ with probability $\frac{D(\vec{p})}{\sum_{\vec{p}\in\mathbf{P}} D(\vec{p})}$
  repeat ▷ K-means algorithm
    $\mathbf{T} \leftarrow \{\vec{c_1}, \vec{c_2}, \cdots, \vec{c_K}\}$
    for $k \leftarrow 1, K$ **do**
      $\mathbf{C_k} \leftarrow$ set of $\vec{p} \in \mathbf{P}$ with $d(\vec{p}, \vec{c_k}) < d(\vec{p}, \vec{c_j})(k \neq j)$
      $\vec{c_k} \leftarrow \frac{1}{|\mathbf{C_k}|}\sum_{\vec{p}\in\mathbf{C_k}} \vec{p}$
  until $\mathbf{T} = \{\vec{c_1}, \vec{c_2}, \cdots, \vec{c_K}\}$ ▷ phasor cluster centroids

To evaluate the performance of our program, we demonstrate image segmentation on FLIM images of fixed cells and living animals acquired with two different FLIM systems. All animal studies in this work were approved by the University of Notre Dame and Indiana University Institutional Animal Care and Use Committees. The first imaging system, phase multiplexing (PM) FLIM, is a custom-built FD-FLIM platform we described in Ref. [13, 14]. Figure 2(a) shows the original two-photon fluorescence intensity image and its corresponding phasor plot of fixed bovine pulmonary artery endothelial (BPAE) cells (FluoCells prepared slide #1, F36924), as well as the clustered phasor plot and segmented images following the K-means clustering algorithm (K=3, Euclidean distance, and replicate=3). We chose K=3 because we had *a priori* knowledge that the BPAE cells were labeled with DAPI (nuclei), MitoTracker Red CMXRos (mitochondria), and Alexa Fluor 488 phalloidin (F-actin). The excitation laser was tuned to 800 nm with a power of 5.0 mW and no emission filter was used. The image was acquired with a pixel dwell time of 20 µs, an image size of 360×360, and was averaged for 10 times. As shown in Fig. 2(a), the K-means clustering approach segmented the image into three structures, i.e., nuclei (red), mitochondria (green), and F-actin (blue). We verified that the segmented images closely matched the fluorophore distributions, indicated by the arrows in Fig. 2(a), by imaging the same sample under a multi-channel commercial two-photon microscope (Nikon A1R-MP) equipped with emission filters

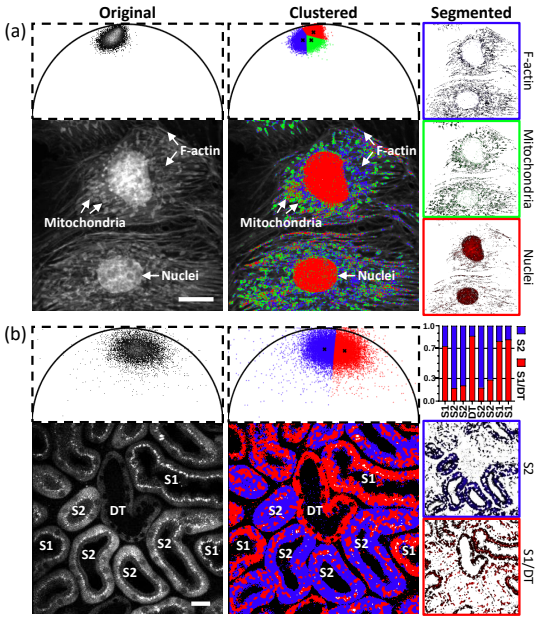

Fig. 2. K-means clustering applied to phasor data acquired with two FLIM systems. (a) Fixed BPAE cells imaged with a custom-built PM-FLIM platform. (b) The kidney in a living mouse imaged with a commercial FD-FLIM system. The stacked bar graph shows the percentages of clustered pixels in the annotated tubules. In the segmented images, the pixels' brightness and hue represent their intensity and cluster color, respectively. Data are representative of $n = 10$ experiments. Scale bar: 20 µm.

corresponding to the three labeling fluorophores (DAPI, MitoTracker, and Alexa Fluor 488) [15]. Since the phasors of the three fluorophores locate closely on the phasor plot, it is challenging to segment them perfectly by either manual selection or K-means clustering. As can be seen in Fig. 2(a), some pixels that belong to the F-actin (blue) structures are incorrectly segmented into the nuclei (red) cluster. Although the segmentation result is not perfect, the K-means clustering approach still outperforms the manual phasor labeling process considering its easiness, speed, and satisfactory segmentation performance.

The second FLIM system is a commercial digital FD-FLIM microscope consisting of an Olympus FV1000-MPE confocal/multiphoton microscope and an ISS FLIM upgrade kit, as described in Ref. [5]. Figure 2(b) shows the original and clustered phasor plots and fluorescence images of the kidney in a living mouse (male C57BL/6J mice at 8-10 weeks of age, obtained from The Jackson Laboratory). The intravital imaging of the mouse kidney was achieved with 800 nm two-photon excitation (12% power), and the endogenous autofluorescence signals were acquired using a 480 nm emission filter (100 nm band width). The image was acquired with a pixel dwell time of 12.5 µs, an image size of 250 × 250, and was averaged for 15-20 times. Due to the weak signals of autofluorescence and low SNR, we applied a 3 × 3 median filter three times on the raw phasor data before performing the clustering algorithm. We have previously verified that the autofluorescence signals came from mouse distal tubules (DT) and proximal tubules (upstream S1 and downstream S2, identified by following the sequential luminal appearance of injected FITC-labeled inulin), as annotated in Fig. 2(b) [5, 16]. Whereas S1 and S2 proximal tubules have distinct metabolic signatures and can be resolved with

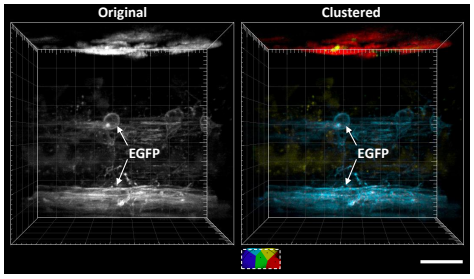

Fig. 3. K-means clustering applied to a 3D phasor stack of a living zebrafish embryo acquired with a custom-built PM-FLIM platform (see Visualization1). Data are representative of $n = 5$ experiments. Scale bar: 20 µm.

FLIM phasors, S1 and DT are remarkably similar in FLIM signatures despite their morphological difference; therefore, we chose K=2 (Euclidean distance, replicate=3) to categorize S1/DT and S2 as two clusters. The segmented images and a stacked bar graph quantifying the percentages of the clustered pixels in the annotated tubules are shown in Fig. 2(b): the S1/DT and S2 tubules are clearly identified and labeled with distinct colors (red for S1/DT, blue for S2) as more than 70% of the pixels in these tubules belong to their labeling clusters.

The K-means clustering approach can also be applied to phasor data of 3D FLIM stacks. Figure 3 shows a 3D FLIM image of a living EGFP labeled *Tg(sox10:megfp)* zebrafish embryo at 2 days post fertilization, acquired with the PM-FLIM platform [13]. The excitation laser was 800 nm with a power of 5.0 mW. No emission filter was used. The stack was acquired with a size of 360 × 360 × 48, a slice depth of 1 µm, a pixel dwell time of 12 µs, and was averaged for 3 times for a better SNR. A 3 × 3 median filter was applied three times to the phasor data before the clustering algorithm. We chose $K = 5$, squared Euclidean, replicate=3 as EGFP and various endogenous fluorophores contributed to the fluorescence signals. Since the 3D stack contains many more pixels, or voxels, the phasor plot can be very crowded, as shown in the inset of Fig. 3, and the manual phasor labeling can be even more challenging. With the K-means algorithm, the phasor clustering and consequently the image segmentation automatically identified and labeled the populations of EGFP (cyan, indicated by arrows) and endogenous fluorophores (other colors) in the 3D stack. Imaris (Bitplane) was used for the 3D reconstruction and visualization. A movie showing the 3D structures of both stacks in Fig. 3 can be found in Visualization1.

Although the K-means clustering approach provides an easy and automatic tool for fluorescence microscopy image segmentation, the K-means clustering itself is an NP-hard optimization problem [7]; therefore, care must be given to the choice of the parameters used in the algorithm. We demonstrate how these parameters, i.e., K, distance metrics, and replicate times, can affect the phasor clustering and image segmentation performances on an intravital mouse kidney image. Figures 4(a) and (b) show that different values of K result in distinct segmentation results. For example, $K = 2$ clearly segments the S1/DT and S2 tubules, as has been shown in Fig. 2(b); $K = 2$ to 4 result in segmentation at subcellular levels and all the segmented images demonstrate distinctive structures of the tubules; when $K \geq 5$, however, the algorithm leads to over-interpretation of the data, as some segmented images capture the same cellular structures (e.g., the cyan and green segments when $K = 5$). We recommend that, if the user has *a priori* knowledge of the number of fluorophores

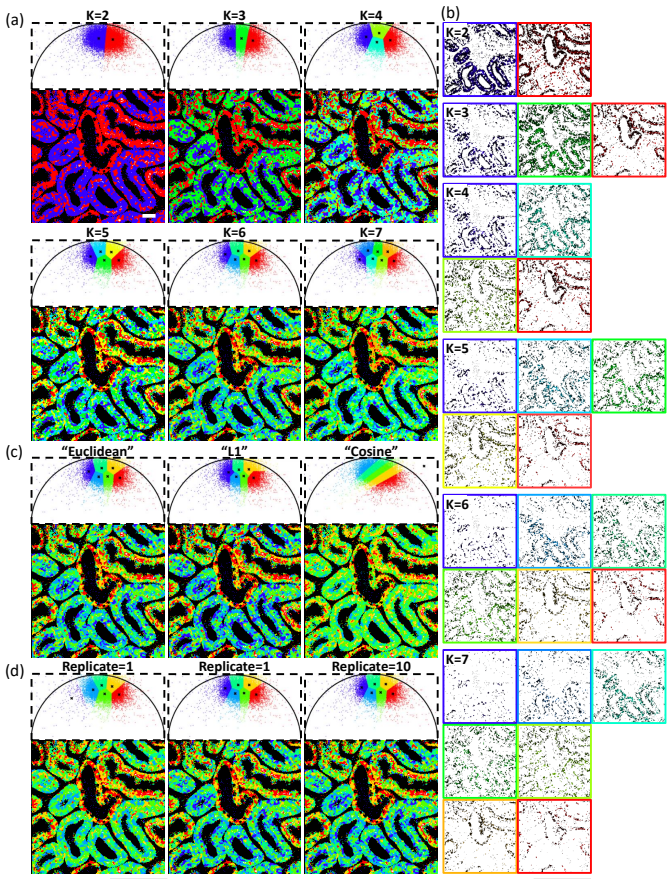

Fig. 4. Parameters in the K-means algorithm can affect the performance of phasor clustering and image segmentation: (a, b) K, the number of clusters; (c) the distance metric; (d) the number of times to replicate the procedure. Scale bar: 20 µm.

presented in the image, then it is appropriate to use that number as K; otherwise, the user could examine the segmented images while increasing the value of K (starting with $K = 2$) using the program. The user should stop increasing K when (1) a satisfactory segmentation result is obtained, or (2) multiple segmented images begin to capture the same cellular structures, as further increase in K does not help segment the image. The definition of distance metrics in the algorithm can also change the segmentation result, as shown in Fig. 4(c). Squared Euclidean and L1 distances show very similar results since the phasor data are two-dimensional; cosine distance, on the other hand, is different as the clustering is solely based on the tangent of the phasor angles, i.e., s_i/g_i, which is proportional to fluorescence (phase) lifetimes; therefore, the clustering with cosine distance is identical to segmenting fluorescence (phase) lifetimes. In order to fully utilize the power of phasors, we recommend the user to use either squared Euclidean or L1 as the distance metric. Finally, we recommend the user to replicate the algorithm at least 3 times because K-means clustering, as an NP-hard optimization problem, could easily converge to a local minimum, as shown in the two different segmentation results for a single replicate in Fig. 4(d); therefore, more repetitions could improve the chance of getting a global minimum, where the total distance between the cluster centroids and the phasor points are the shortest.

Owing to the two-dimensional nature of phasor data, the execution of the program is fast. Using a personal computer with 2.20 GHz Intel Core i7-8750H CPU and 32 GB RAM, the K-means clustering program's execution time for the 250 × 250, 360 × 360 (Fig. 2), and 360 × 360 × 48 (Fig. 3) images were 1.33 s, 2.28 s, and 54.59 s, respectively (average of 10 runs; $K = 4$, Euclidean distance, replicate=3). Note that, in principle, the K-means algorithm may be applied to other types of FLIM data, such as the raw temporal decay histograms in TCSPC with, e.g., 256 time channels [9]. However, the K-means algorithm could be extremely slow and fail to converge if applied to 256-dimensional data; moreover, unlike the two-dimensional phasor data, the clustering of 256-dimensional data is hard to visualize.

In conclusion, we have presented a novel and unbiased approach to automatically segment fluorescence microscopy images into sensible structures by applying the K-means clustering algorithm to FLIM phasors. We have also provided an open-source, user-friendly program that allows easy access to this approach. The approach has been successfully demonstrated on 2D and 3D FLIM data of fixed cells and living animals acquired with two different FLIM systems. Although not shown here, we have verified that the K-means approach can also identify groups of the same fluorophores with different ratios of species. We believe this approach could be a powerful new tool for FLIM researchers who can easily import their phasor data into the program and gain insights from the new segmentation results.

FUNDING.

National Science Foundation (NSF) (CBET-1554516).

ACKNOWLEDGMENT.

Zhang's research was supported by the Berry Family Foundation Graduate Fellowship of Advanced Diagnostics & Therapeutics (AD&T), University of Notre Dame. Animal care support from Alfred P. Sloan Foundation (C.J.S.).

REFERENCES

1. M. Y. Berezin and S. Achilefu, Chem. Rev. **110**, 2641 (2010).
2. G. Weber, J. Phys. Chem. **85**, 949 (1981).
3. Y. Sun, R. N. Day, and A. Periasamy, Nat. Protoc. **6**, 1324 (2011).
4. S. Ranjit, L. Malacrida, D. M. Jameson, and E. Gratton, Nat. Protoc. **13**, 1979 (2018).
5. T. Hato, S. Winfree, R. Day, R. M. Sandoval, B. A. Molitoris, M. C. Yoder, R. C. Wiggins, Y. Zheng, K. W. Dunn, and P. C. Dagher, J. Am. Soc. Nephrol. **28**, 2420 (2017).
6. J. Macqueen, Proc. Fifth Berkeley Symp. on Math. Stat. Probab. **1**, 281 (1967).
7. A. K. Jain, Pattern Recogn. Lett. **31**, 651 (2010).
8. P. T. C. So, T. French, W. M. Yu, K. M. Berland, C. Y. Dong, and E. Gratton, Bioimaging. **3**, 49 (1995).
9. W. Becker, J. Microsc. **247**, 119 (2012).
10. Y. Zhang, G. D. Vigil, L. Cao, A. A. Khan, D. Benirschke, T. Ahmed, P. Fay, and S. S. Howard, Opt. Lett. **42**, 155 (2017).
11. Y. Zhang, A. A. Khan, G. D. Vigil, and S. S. Howard, J. Opt. Soc. Am. A **33**, B1 (2016).
12. D. Arthur and S. Vassilvitskii, Proc. Eighteenth Annu. ACM-SIAM Symp. on Discret. Algorithms **8**, 1027 (2007).
13. Y. Zhang, I. H. Guldner, E. L. Nichols, D. Benirschke, C. J. Smith, S. Zhang, and S. S. Howard, Proc. SPIE **10882** (2019).
14. Y. Zhang, D. Benirschke, O. Abdalsalam, and S. S. Howard, Biomed. Opt. Express **9**, 4077 (2018).
15. Y. Zhang, Y. Zhu, E. Nichols, Q. Wang, S. Zhang, C. Smith, and S. Howard, IEEE Conf. on Comput. Vis. Pattern Recognit. (2019).
16. R. Kalakeche, T. Hato, G. Rhodes, K. W. Dunn, T. M. El-Achkar, Z. Plotkin, R. M. Sandoval, and P. C. Dagher, J. Am. Soc. Nephrol. **22**, 1505 (2011).

FULL REFERENCES

1. M. Y. Berezin and S. Achilefu, "Fluorescence lifetime measurements and biological imaging," Chem. Rev. **110**, 2641–2684 (2010).
2. G. Weber, "Resolution of the fluorescence lifetimes in a heterogeneous system by phase and modulation measurements," J. Phys. Chem. **85**, 949–953 (1981).
3. Y. Sun, R. N. Day, and A. Periasamy, "Investigating protein-protein interactions in living cells using fluorescence lifetime imaging microscopy," Nat. Protoc. **6**, 1324–1340 (2011).
4. S. Ranjit, L. Malacrida, D. M. Jameson, and E. Gratton, "Fit-free analysis of fluorescence lifetime imaging data using the phasor approach," Nat. Protoc. **13**, 1979–2004 (2018).
5. T. Hato, S. Winfree, R. Day, R. M. Sandoval, B. A. Molitoris, M. C. Yoder, R. C. Wiggins, Y. Zheng, K. W. Dunn, and P. C. Dagher, "Two-photon intravital fluorescence lifetime imaging of the kidney reveals cell-type specific metabolic signatures," J. Am. Soc. Nephrol. **28**, 2420–2430 (2017).
6. J. Macqueen, "Some methods for classification and analysis of multivariate observations," Proc. Fifth Berkeley Symp. on Math. Stat. Probab. **1**, 281–297 (1967).
7. A. K. Jain, "Data clustering: 50 years beyond K-means," Pattern Recogn. Lett. **31**, 651–666 (2010).
8. P. T. C. So, T. French, W. M. Yu, K. M. Berland, C. Y. Dong, and E. Gratton, "Time-resolved fluorescence microscopy using two-photon excitation," Bioimaging. **3**, 49–63 (1995).
9. W. Becker, "Fluorescence lifetime imaging - techniques and applications," J. Microsc. **247**, 119–136 (2012).
10. Y. Zhang, G. D. Vigil, L. Cao, A. A. Khan, D. Benirschke, T. Ahmed, P. Fay, and S. S. Howard, "Saturation-compensated measurements for fluorescence lifetime imaging microscopy," Opt. Lett. **42**, 155–158 (2017).
11. Y. Zhang, A. A. Khan, G. D. Vigil, and S. S. Howard, "Investigation of signal-to-noise ratio in frequency-domain multiphoton fluorescence lifetime imaging microscopy," J. Opt. Soc. Am. A **33**, B1–B11 (2016).
12. D. Arthur and S. Vassilvitskii, "K-means++: the advantages of careful seeding," Proc. Eighteenth Annu. ACM-SIAM Symp. on Discret. Algorithms **8**, 1027–1025 (2007).
13. Y. Zhang, I. H. Guldner, E. L. Nichols, D. Benirschke, C. J. Smith, S. Zhang, and S. S. Howard, "Three-dimensional deep tissue multiphoton frequency-domain fluorescence lifetime imaging microscopy via phase multiplexing and adaptive optics," Proc. SPIE **10882** (2019).
14. Y. Zhang, D. Benirschke, O. Abdalsalam, and S. S. Howard, "Generalized stepwise optical saturation enables super-resolution fluorescence lifetime imaging microscopy," Biomed. Opt. Express **9**, 4077–4093 (2018).
15. Y. Zhang, Y. Zhu, E. Nichols, Q. Wang, S. Zhang, C. Smith, and S. Howard, "A Poisson-Gaussian denoising dataset with real fluorescence microscopy images," IEEE Conf. on Comput. Vis. Pattern Recognit. (2019).
16. R. Kalakeche, T. Hato, G. Rhodes, K. W. Dunn, T. M. El-Achkar, Z. Plotkin, R. M. Sandoval, and P. C. Dagher, "Endotoxin uptake by S1 proximal tubular segment causes oxidative stress in the downstream S2 segment," J. Am. Soc. Nephrol. **22**, 1505–1516 (2011).